Construction of a Computer Model to Investigate Sawtooth Effects in the Purkinje System

Edward J. Vigmond*, *Member, IEEE*, and Clyde Clements

***Abstract*—The sawtooth effect refers to how one end of a cardiac cell is depolarized, while the opposite end is hyperpolarized, upon exposure to an exogenous electric field. Although hypothesized, it has not been observed in tissue. The Purkinje system is a one-dimensional (1-D) cable-like system residing on the endocardial surface of the heart and is the most obvious candidate for the manifestation of this phenomenon. This paper describes a computer modeling study of the effect of electric fields on the Purkinje system. Starting with a three-dimensional geometrically realistic, finite element, ventricular description, a Purkinje system is constructed which adheres to general physiological principles. Electrical activity in the Purkinje is described by use of 1-D cubic Hermite finite elements. Such a formulation allows for accurate modeling of loading effects at the Purkinje-myocyte junctions, and for preserving the discrete nature of the system. The response of a strand of Purkinje cells to defibrillation strength shocks is computed under several conditions. Also, the response of the isolated Purkinje network is illustrated. Results indicate that the geometry of the Purkinje system is the greatest determinant for far field excitation of the system. Given parameters within the plausible physiological range, the 1-D nature of the Purkinje system may lead to sawtooth potentials which are large enough to affect excitation. Thus, the Purkinje system is capable of affecting the defibrillation process, and warrants further experimentation to elucidate its role.**

***Index Terms*—Cardiac electrophysiology, computer modeling, defibrillation, finite elements, Purkinje system.**

I. Introduction

ONCE a heart begins to fibrillate, the only known therapy is the application of a large electric shock, delivered either via surface electrodes or via implantable defibrillators. Despite the proven success of this technique, many questions regarding the basic physical processes remain unelucidated. Of particular note is the lack of information regarding the role that the heart's fast conduction system, the Purkinje network, plays in the defibrillation process.

Its role in defibrillation is not clear since it cannot be assumed that it will be excited in the same manner as the myocardium for several reasons. Even though the myocardium can be optically mapped during defibrillation strength shocks, the Purkinje network is so fine that its response lies below the resolution of optical recording devices when recording on the organ level. The Purkinje system runs on top of, and is isolated from the myocardium except at the Purkinje Myocyte Junctions (PMJs). The response of tissue to an extracellular stimulus is dependent on the angle that the applied field makes with the fiber direction of the tissue, as well as how the conductivity changes [1]. The Purkinje system conductivity is defined by its local tangential direction, and this direction is unrelated to the myocardial conductivity tensor upon which it is laid. Furthermore, the fibers of the Purkinje system make abrupt turns and run in all directions. Electrophysiologically, cells in the Purkinje system have a different channel expression than ventricular myocytes [2] as well as distinct geometry [3], leading to different responses to the same shock strength [4]. Thus, the excitation pattern of the Purkinje system will be distinct from that of the myocardium.

The sawtooth effect has been hypothesized to exist in cardiac tissue as a mechanism to explain the excitation of tissue far from stimulating electrodes, where the field would otherwise be too weak to raise the transmembrane voltage above threshold [5]–[7]. The basis for it lies in the discrete nature of the coupling between myocytes, assuming that the gap junction resistance is quite large compared to the longitudinal intracellular resistance of a myocyte. Such a resistance, theoretically, allows for the development of large voltage drops across the gap junction, with one end of the cell hyperpolarized and the opposite depolarized. This phenomenon manifests itself as a periodic sawtooth variation imposed upon a smoothly varying potential. These perturbations have been calculated to be of sufficient magnitude to exceed threshold far from the stimulating electrodes. While this effect has been demonstrated experimentally in isolated cell pairs [8], attempts to observe it in tissue have failed [9]. This failure has been attributed to the many lateral gap junctions in a single cell which lessen the abrupt coupling. Since the Purkinje system is one-dimensional (1-D) [10], meaning that at any point, current flow exists only in one direction, it will not suffer from this dampening, making it an ideal candidate for manifestation of the sawtooth effect.

There have been few computer models of the Purkinje system [11], [12], and those presented have not been used for extracellular stimulation. To properly account for the sawtooth effect and loading at the PMJs, a mathematical formulation which incorporates longitudinal current flow must be considered. Cubic Hermite finite elements are suitable for such a purpose as they are based upon solving the potential and its gradient at each node of the solution space. Furthermore, discretization can be per-

Manuscript received May 31, 2006; revised August 8, 2006. This work was supported by the Natural Sciences and Engineering Research Council of Canada, MITACS, and the Alberta Ingenuity Fund. *Asterisk indicates corresponding author.*

*E. Vigmond is with the Department of Electrical and Computer Engineering, University of Calgary, Calgary, AB T2N 1N4, Canada (e-mail: vigmond@ucalgary.ca).

C. Clements is with the Department of Electrical and Computer Engineering, University of Calgary, Calgary, AB T2N 1N4, Canada.

Color versions of Figs. 1 and 3–6 are available online at http://ieeexplore.ieee.org.

Digital Object Identifier 10.1109/TBME.2006.888817

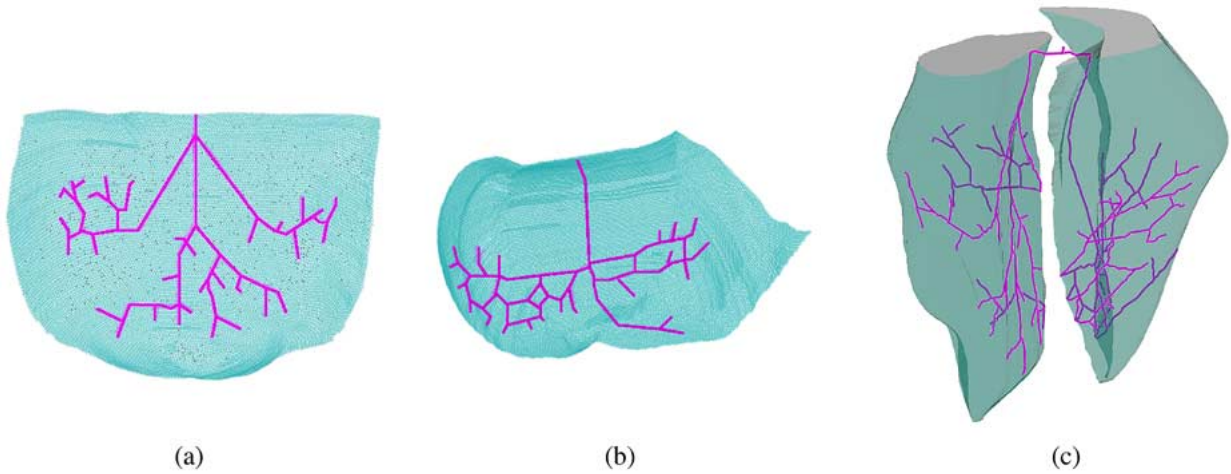

Fig. 1. (a) Unrolled left endocardium, (b) unrolled right endocardium, and (c) 3-D His-Purkinje system and endocardial surfaces. The left endocardium is on the left.

formed at the single cell level and discrete resistances between the elements can be incorporated, making it a natural choice for accurately modeling the system.

This paper describes the development of an anatomically accurate Purkinje network which is based on 1-D cubic Hermite finite elements. Its unique features include current conservation at bifurcations and discrete junctional resistances. The formulation will be verified to produce the proper results by comparison with linear elements. To understand factors affecting the development of sawtooth potentials, a straight Purkinje fiber will be subjected to various fields, and model parameters varied. An anatomically realistic network will then be exposed to different fields to determine excitation patterns.

II. Methods

A. Geometrical Construction Overview

To construct the Purkinje network, a tetrahedral finite element model based on the San Diego rabbit heart model [13] was used as the starting point The endocardial surfaces were extracted, resulting in two triangularly meshed surfaces (see Fig. 1). To construct a Purkinje conduction system, the following were performed.

1) The ventricular endocardial surfaces were flattened onto a plane using a multidimensional scaling technique [14] which attempted to preserve geodesic distances. Distances were computed by the classic Dijkstra algorithm [14], [15].
2) A conduction system was manually laid out on each of the endocardial surfaces. This was based on schematics and pictures of the conduction system, text descriptions of heart anatomy, and excitation mappings of the heart [12], [16]–[19]. As there was a high degree of variability among these sources, the important features were implemented. In particular, the left Purkinje network had three major areas of activation: the septum, the inferior free wall, and the superior free wall. In the right Purkinje network, the activation proceeded primarily from the septum out to the papillary muscles in the lower part of the ventricle. For each ventricle, a single cable descended from the base and proceeded apically. At appropriate places, daughter branches were added which ran towards the areas of early activation. The major bifurcation points were chosen to roughly correspond to published descriptions. More cables were added to provide better coverage for activation.
3) The two-dimensional (2-D) representation of the Purkinje network was then mapped to three-dimensional (3-D) space. Step 1) provided us with a one-to-one mapping of the 3-D mesh points to a set of 2-D points. The inverse of this mapping was used in Step 3). With the 3-D mappings determined, the left and right Purkinje networks were joined to form a common point of origin, and a segment representing the bundle of His was added.
4) The endpoints of the Purkinje networks (i.e., those points that make electrical contact with—and activate—the ventricular myocardium) were inserted into the ventricular wall. Each cable end was extended into the myocardium by appending elements. The new elements made an angle of approximately 45° with the surface tangent to avoid any sharp discontinuities, and continued for several hundred micrometers into the tissue. No new nodes were generated.

B. Mathematical Basis

Assume that the extracellular potential, ϕ_e, is due to the bulk myocardium only, i.e., we ignore the field produced by the Purkinje system. Also assume we have knowledge of the spatial and temporal derivatives of the potential, i.e., $\partial\phi_e/\partial x$, $\partial\phi_e/\partial t$, and $\partial^2\phi_e/\partial x\partial t$ are all known. We also require the intracellular potential, ϕ_i, and its gradient, $\partial\phi_i/\partial x$, at the beginning of the time step. The longitudinal current is given by

$$i_L = -\pi\rho^2\sigma_i\frac{\partial\phi_i}{\partial x} \tag{1}$$

where ρ is the radius of the Purkinje fiber, and σ_i is the intracellular conductivity.

The governing parabolic equation is given by

$$\nabla \cdot \overline{\sigma}_{\mathrm{i}} \nabla \phi_i = \beta \left(C_m \frac{\partial V_m}{\partial t} + I_{\mathrm{ion}}(V_m, \bar{\zeta}) \right) \tag{2}$$

with $V_m = \phi_i - \phi_e$, and $\bar{\zeta}$ is a set of variables describing the state of the membrane. The DiFrancesco-Noble model of the Purkinje cell [20] was used with the maximum sodium conductance increased by a factor of 3 compared to the published value. Although studies usually increase the sodium conductance by a factor of 1.5 [21], [22], conductance was further augmented to increase the propagation velocity.

To determine V_m, we recognize that the cells are connected by gap junctions, which are represented as resistors [see Fig. 2(a)]. ϕ_i is defined as the potential midway along the gap junction, and V_m at either end of the junction can be expressed using the longitudinal current

$$V_m^{\pm} = \phi_i - \phi_e \mp i_L \frac{r_{gj}}{2} \tag{3}$$

where r_{gj} is the gap junction resistance. Thus, after determining V_m at the ends of each cell along the cable, we split the operator to isolate the ionic current term and apply first-order differencing in time, allowing an update of V_m based on ionic current flow

$$\Delta V_m = -\frac{\Delta t}{C_m} I_{\mathrm{ion}} \tag{4}$$

ϕ_i and i_L are then recomputed at each junction from

$$\phi_i = \frac{V_m^+ + V_m^-}{2} + \phi_e \tag{5}$$

$$i_L = \frac{V_m^+ - V_m^-}{r_{gj}}. \tag{6}$$

The rest of the operator considers longitudinal current flow. Using an implicit method and first-order differencing in time

$$\nabla \cdot \sigma_i^* \nabla \phi_i^{t+1} = \kappa \left(\phi_i^{t+1} - \phi_i^t - \phi_e^t + \phi_e^{t-1} \right) \tag{7}$$

where σ_i^* is the equivalent conductivity which lumps σ_i and r_{gj} (see the Appendix), and $\kappa = \beta C_m / \Delta t$.

Applying the finite element method (see the Appendix for details) and collecting the unknowns on the left-hand side

$$(\kappa \mathbf{M} - \mathbf{K}) \boldsymbol{\phi_i^{t+1}} = \kappa \mathbf{M} \left(\boldsymbol{\phi_i^t} + \boldsymbol{\Delta \phi_e} \right) \tag{8}$$

where $\mathbf{M}$ and $\mathbf{K}$ are the mass and stiffness matrices, respectively. Each vector is composed of the labeled quantity and its spatial derivative. In particular, the intracellular potential vector contains the following quantities:

$$\boldsymbol{\phi_i} = [\phi_i(x_1) \ \ldots \ \phi_i(x_n) \ i_L(x_1) \ \ldots \ i_L(x_n)]^T \tag{9}$$

At each bifurcation, current conservation is enforced. Assuming that the right end of element a is the parent of elements b and c, the usual finite element equation associated with the derivative of the potential at the right end of element a is replaced with

$$i_{L,a} = i_{L,b} + i_{L,c} \tag{10}$$

The Purkinje system is coupled to the bulk myocardium through Purkinje-Myocyte Junctions (PMJs) which are represented as fixed resistances (R_{PMJ}). At the cable ends, current flow through through the PMJ is enforced as a boundary condition. For a cable end at x_e

$$i_L = \sum_k \frac{\phi_i(x_e) - \phi_i^M(x_k)}{R_{\mathrm{PMJ}}} \tag{11}$$

where $\phi_i^M(x)$ is an intracellular potential in the bulk myocardium, and k is the set of indices of the myocytes to which the Purkinje cell is connected.

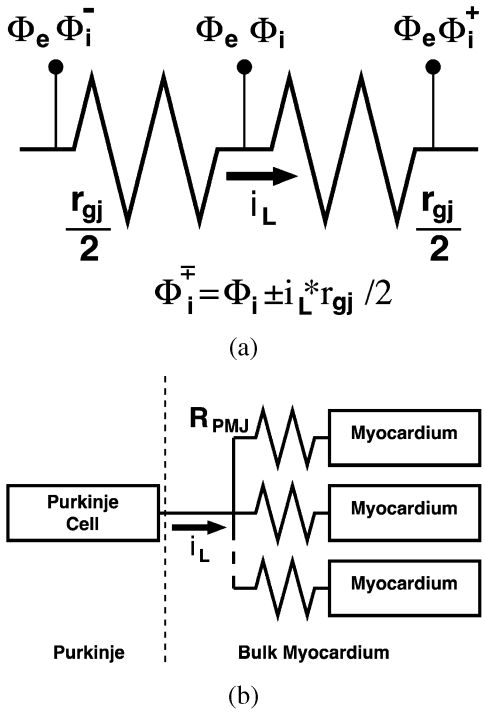

Fig. 2. (a) The intracellular potential at the midpoint of the gap junction is denoted by Φ_i, on the left by Φ_i^- and on the right by Φ_i^+. The gap junction length is so small that the extacellular potential, Φ_e, is constant across the junction. The current flowing through the junction of resistance r_{gj} is i_L. (b) Purkinje-Myocyte junction: A single Purkinje cell can be connected to multiple myocytes via gap junctions, each with resistance R_{PMJ}. The current flowing from the Purkinje cell into myocardium, i_L, is implemented as a boundary condition when solving the Purkinje system activity, while it is treated as a stimulus current for the myocardial solution.

III. Results

Calculation of the geodesic distances was a CPU intensive task. The right endocardial surface contained 17092 vertices and 33984 triangles; it required approximately 8 h of CPU time to compute all geodesic distances. The left endocardial surface contained 13529 vertices, 26916 triangles, and required 4 h of CPU time for determination of the geodesic distances. All

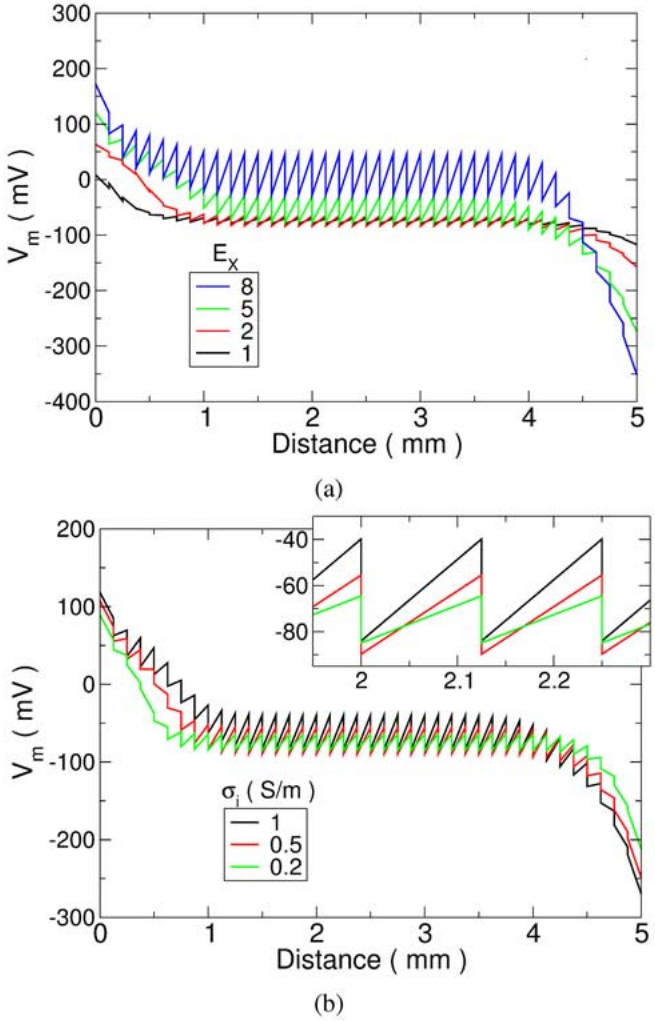

Fig. 3. Transmembrane voltage responses along a 5-mm-long cable, 1 ms after the application of a constant electric field oriented along the cable axis. Gap junction resistances were 1 $\mathrm{M}\Omega$. (a) The shock strength is indicated in V/cm. The effective conductivity was constant at 0.3 S/m. (b) For a field of strength 5 V/cm, transmembrane voltage is shown for several intracellular conductivities, indicated in S/cm. The inset shows a detail over the central region.

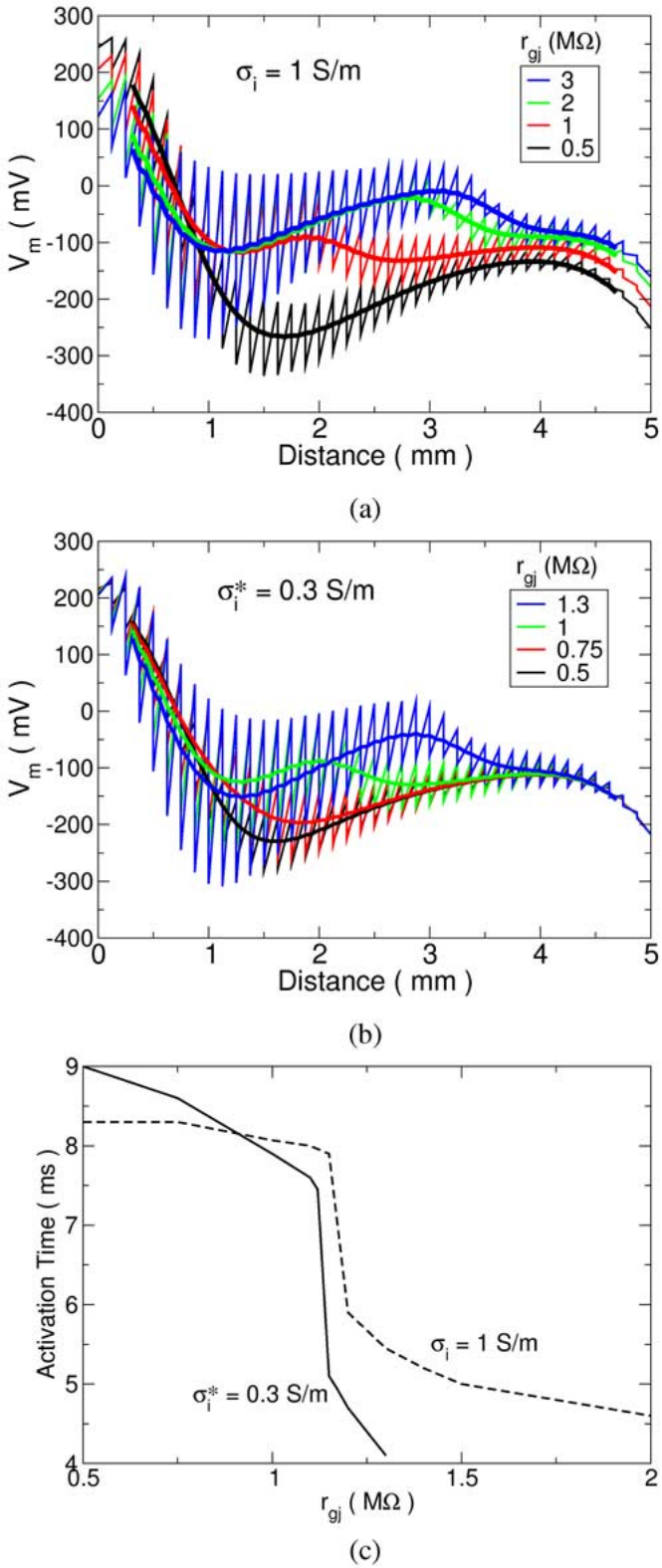

Fig. 4. Transmembrane voltage responses along a 5-mm-long cable, 1 ms after the onset of a point stimulus located 1 mm above the end. Gap junction resistances, r_{gj}, are indicated in $\mathrm{M}\Omega$. (a) Intracellular conductivity was constant at 1 S/m. (b) The effective conductivity of the cable was constant at 0.3 S/m. The baseline is indicated by a solid line. (c) Time for the entire fiber to activate as a function of gap junction resistance for (a) and (b).

geodesic computations were performed on a computer running Linux with a 1.6 GHz Opteron processor.

Application of the scaling procedure required 2.5 h and 1 h of CPU time for the right and left endocardial surfaces, respectively. The flattened surfaces are shown in Fig. 1. Mapping the 2-D Purkinje network into 3-D required only a couple of minutes of CPU time. The final result is shown in Fig. 1(c).

A. Stimulation of a Straight Fiber With Constant Field

A set of simulations was performed for a 5-mm-long, straight cable of radius 10 $\mu\mathrm{m}$ [3] immersed in an infinite bath of conductivity 1 S/cm. The length of each cell was 125 $\mu\mathrm{m}$ [3]. Results are shown in Fig. 3(a) for a constant field of several defibrillation strengths, ranging from 1 to 8 V/cm. There is a basic excitation pattern, with depolarization at one end and hyperpolarization at the other. The cable is sufficiently long so that the middle region is unaffected by end effects. Along this middle portion, there is a constant baseline amplitude upon which a sawtooth variation in potential is superimposed. For the field strengths of 1, 2, 5, and 8 V/cm, the corresponding

sawtooth amplitudes were 9.2, 18.6, 46.2, and 74.5 mV, respectively. Thus, the sawtooth amplitude was linearly related to the field strength. The sawtooth amplitude was largest over the middle region where the intracellular longitudinal current was largest. For fields less than 2 V/cm, the results fall on the 2 V/cm line but have decreased oscillations about the baseline. As the field was increased, the middle region of the cable became more depolarized in a highly nonlinear manner. Defining the baseline as the average of the minimum and maximum sawtooth amplitudes, the baselines were −74.9, −74.8, −55.2, and 9 mV for the four field strengths. Below 2 V/cm, the baseline was constant but increased dramatically with field strength beyond that.

The intracellular conductivity, σ_i, was next varied from 0.2 to 1 S/m to assess its impact on induced transmembrane potentials. The gap junction resistance was fixed at 1 $\mathrm{M}\Omega$, and a constant electric field of 2 V/m was applied along the cable axis. Results are seen in Fig. 3(b). As the conductivity was increased, the sawtooth amplitude increased, and the baseline increased. For smaller conductivities, there was essentially no increase in the baseline in the middle region, only 1.5 mV, but for the largest conductivities, the baseline was about 10 mV more depolarized in the central region of the cable. The sawtooth amplitude increased by just over a factor of two, from 20 to 44 mV, over a five-fold increase in conductivities. The space constant increased with the conductivity value, as can be seen by the larger region affected at the ends of the cable with higher conductivity values.

B. Stimulation of a Straight Fiber With a Point Source

Since the gradient of the extracellular field is often shown as being important for field stimulation, a set of simulations was conducted for a point source stimulus, which has a gradient in the electric field unlike the previous field used. A monopole of strength -100 μA was positioned 1 mm over the end of the cable, and the transmembrane response computed for gap junction resistances ranging from 0.5 to 3 $\mathrm{M}\Omega$ (see Fig. 4). Two sets of simulations were performed, one in which σ_i was held constant [see Fig. 4(a)] and one in which the effective intracellular conductivity, σ_i^*, was kept constant [see Fig. 4(b)]. A value of 0.3 S/m was chosen for σ_i^*, which is larger than previous studies [22], because faster propagation was desired [23]. The objective of the former set of simulations was to simulate experimental manipulation of gap junctional conductances by application of octanol or heptanol. The latter set was to demonstrate the range of behavior possible as could be determined by estimating σ_i^* from propagation velocity measurements, but not knowing how the effective conductivity was distributed.

For constant σ_i, there was depolarization below the point source, as expected, and hyperpolarization at the opposite end. The voltage was monotonic along the length of the cable, with an initial local minimum around 1.5 mm for r_{gj} of 0.5 $\mathrm{M}\Omega$, and at least one local maximum occurring at some point after that. There were significant differences in the depolarization pattern as the gap junctional resistance was increased. Part of the difference was due to the change in space constant of the cable which is dependent on σ_i^*. This effect can be seen in the rate of the initial drop off in depolarization, which is faster for higher resistances. As previously observed, increasing the resistance increased the amplitude of the sawtooth variation in voltage. For resistances greater than or equal to 1 $\mathrm{M}\Omega$, a new secondary local maximum appeared in the baseline. Decreasing r_{gj} below 0.5 $\mathrm{M}\Omega$ had very little effect. This maximum increased with increasing r_{gj} and occurred farther along the cable. This secondary depolarization maximum could lead to the transmembrane voltage exceeding threshold, resulting in action potentials originating from the point of the secondary maximum as well as the proximal portion of the cable.

Fixing the effective conductivity kept the space constant of the cable fixed. The initial decay along the cable was the same for all gap junction resistances. Like the preceding set of simulations, increasing r_{gj} resulted in a secondary depolarization maximum that increased in amplitude and distance along the cable with increasing resistance. The maximum gap junction resistance that could be used was limited in this set of simulations to about 1.3 $\mathrm{M}\Omega$, the point at which σ_i would have to be infinite to maintain the desired σ_i^*.

The time for the entire cable to activate was measured [see Fig. 4(c)] for both sets of simulations described above. As the resistance was increased, there was initially a small decrease in activation time. This was more dramatic for constant σ_i^* than constant σ_i. The initial portion of the cable was directly activated by the stimulus and the rest of cable was activated by propagated activity from this region. As the resistance was increased, the initial segment would reach threshold more quickly as well as a larger segment would be depolarized, resulting in quicker activation of the whole cable. When the resistance increased enough to cause the secondary maximum to exceed threshold, the activation time was reduced dramatically. For both situations, this occurred around 1.17 $\mathrm{M}\Omega$. At this level of gap junctional coupling, the secondary depolarization reached threshold and activation proceeded outward from there, as well as from the initial portion of the cable. As the resistance was increased, the activation time decreased because the location of the secondary depolarization moved farther along the cable. The slope in this region of the graph was much steeper than in the initial region indicating that there was much more variability in the location of the secondary depolarization than there was in the size of the proximal region affected directly by the stimulus.

C. Isolated Purkinje Network

The angle of incidence of an electric field upon a fiber determines the strength of the interaction, so it was presumed that the His/Purkinje network with all its variously oriented branches, would respond differently to the various fields. The isolated Purkinje system was subject to 1-ms constant electric fields of 5 V/cm in the three principal directions. As expected, the excitation patterns for each of the fields were quite distinct (see Fig. 5). Many small regions were affected strongly. These regions corresponded to either endings or sharp curves, while straight regions were relatively unaffected, demonstrating once again that sawtooth effects are not strong under constant electric fields. Excitation occurred downfield where there were abrupt changes in conductivities. Such changes encompassed bends in the branches and endings. Conversely, deexcitation occurred upfield, again at abrupt changes in geometry. Thus, looking at a

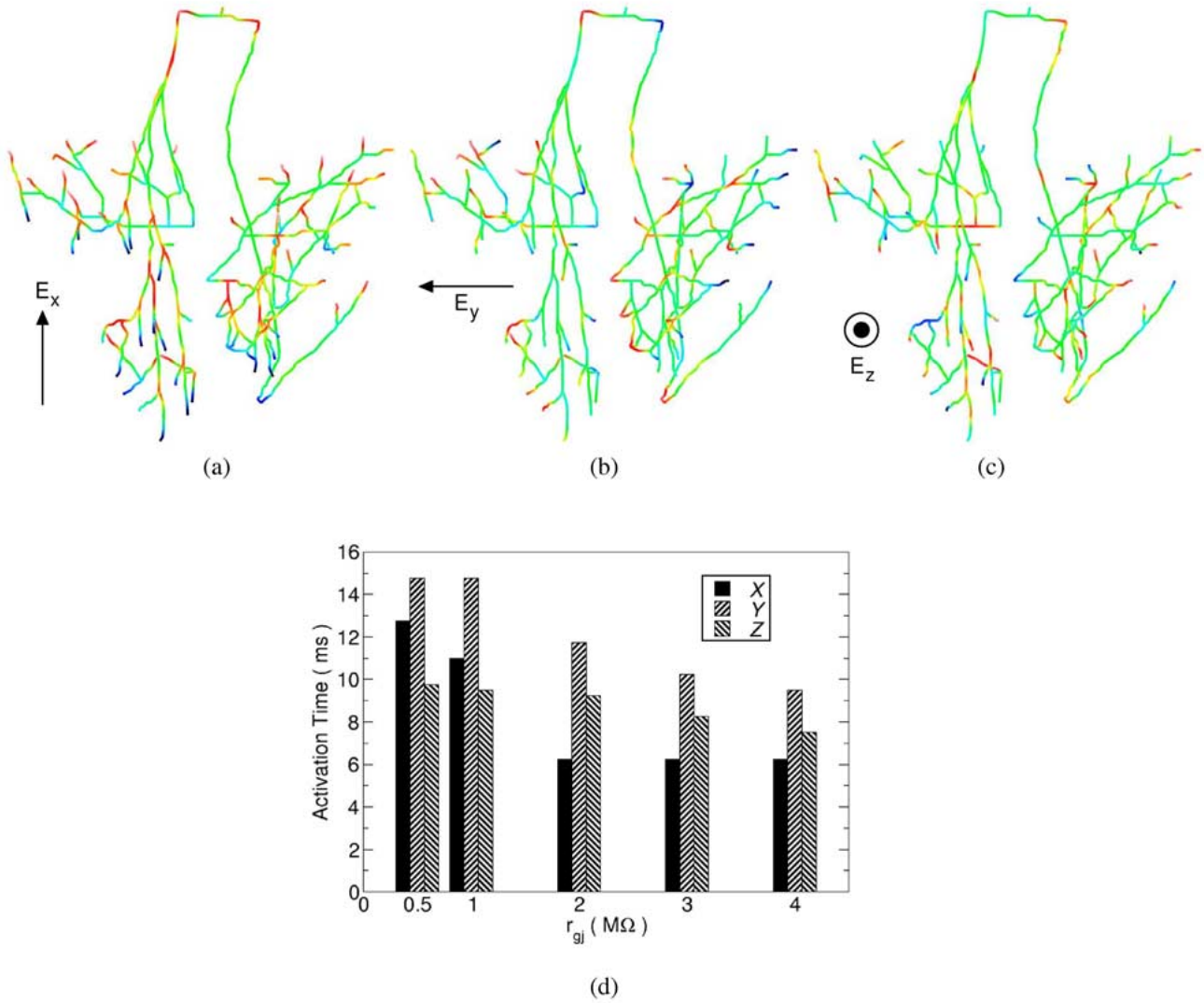

Fig. 5. Electric field stimulation of an isolated Purkinje system. Constant electric fields were applied in the (a) x, (b) y, and (c) z directions. Induced transmembrane voltages are shown 1.25 ms after application of the field. The color scale goes from -190 (black) to 60 (red) mV. (d) The time for the entire tree to activate as a function of the gap junction resistance. The legend indicates the direction of the electric field.

field in the x-direction Fig. 5(a), the bottom ends of the network are hyperpolarized while the tops are depolarized. For the other directions, similar patterns hold in the appropriate directions. A field along the x-direction appeared to activate more of the network than fields oriented along the other directions.

The time for the entire network to activate is given in Fig. 5(d). This time varied with the direction of the field, and decreased with increasing gap junction resistance. Decreasing r_{gj} below 0.5 $\mathrm{M}\Omega$ had essentially no effect. The total activation time was determined by the lengths of the branches which were unaffected by the stimuli. The vast majority of the network was excited within 6 ms with a particular branch being responsible for the remaining time. Such branches relied on activity to propagate into them, and took considerably longer to activate than branches which were field stimulated at both ends. The activation time reduced drastically for small increases in coupling resistance if that change in resistance resulted in field activation of a new branch, otherwise the decrease in activation time was small with an increase in r_{gj}. Fields along the y-direction took the longest time to activate the network while fields in the x-direction excited the entire network faster. For the most part, increasing the gap junction resistance had a gradual effect, reducing the activation time by slightly increasing the regions depolarized by the field. The sawtooth potential was enough to bring a near threshold excitation portion of the membrane above threshold. With an x-directed field, there was a drastic decrease in excitation time as the resistance was increased from 1 to 2 $\mathrm{M}\Omega$. This corresponded to a case where the sawtooth effect became large enough to trigger a branch that was raised to near threshold by the field. If the field failed to trigger the branch, the branch would be activated by activity propagating through the Purkinje network.

D. Ventricular Activation

Last, the method was demonstrated to work with the ventricular finite element model of the ventricles from which the tree was derived. The Beeler-Reuter equations as modified by Druhard and Roberge [24] were used to model the ventricular

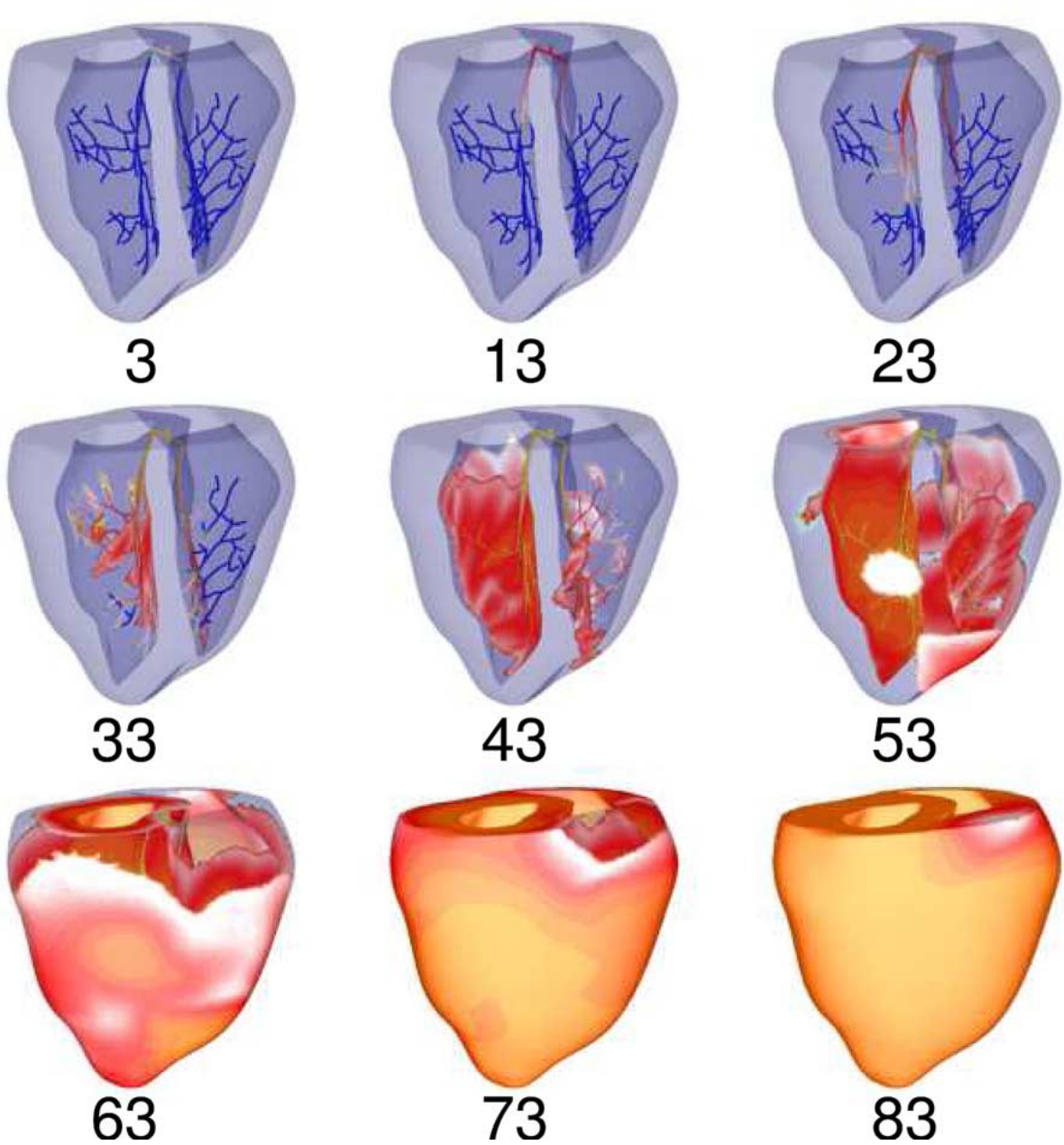

Fig. 6. Activation of the ventricles by the Purkinje system. Only the Purkinje system, the endocardium and the endocardium are shown. Colors indicate transmembrane voltage with blue representing -90 mV and white representing all voltages above 10 mV. The time since His stimulation is indicated in milliseconds.

membrane. Activation of the ventricles is depicted in Fig. 6. The proximal 5 segments of the His bundle were stimulated intracellularly and the ensuing propagation allowed to develop. Coupling resistances at the PMJs were set to 1 $\mathrm{M}\Omega$. Setting this value too high ($>\approx 100\ \mathrm{M}\Omega$) or too low ($<\approx 10\ \mathrm{M}\Omega$) would result in failed propagation due to either insufficient current into the myocardium, or too much loading of the Purkinje cell, respectively. There was a noticeable propagation delay of several milliseconds across the PMJ, as seen experimentally [25]. with the exact delay depending on local loading effects. Activation of the ventricles took about 80 ms for completion, starting from the intial bundle of His stimulation, with activity proceeding generally from endocardium to epicardium, apex to base. Note the epicardial breakthrough patterns as observed experimentally.

IV. Discussion

A. Modeling Technique

This paper described the construction of a unique, anatomically realistic Purkinje network. It implements the following features: 1) It is subject to extracellular field stimulation. The fibers follow smooth courses so they will not experience spurious excitations at nonphysiological corners. Thus, it is the only model to date appropriate for defibrillation studies; 2) It is cou-

pled to a bidomain model of the ventricles through PMJs, allowing for the proper activation and interaction of the two systems; 3) It preserves the discrete nature of the cells and, thus, makes possible the study of the sawtooth phenomenon; 4) Because it uses cubic Hermite elements, it properly accounts for current flow since that is a quantity explicitly solved for. Hence, at the PMJs, proper loading is taken account, as well as at any bifurcations; 5) Model parameters are introduced in a direct and natural way. For example, gap junctions are kept as discrete entities without need for spatial distribution, while conductivities are kept as distributed. Resistances, radii, and cell lengths may be all set on an individual cell basis without increasing storage or complexity; 6) longer cell lengths are less of an issue than with linear elements. When laying the Purkinje tree on the endocardium, no new nodes were introduced but, keeping the cables running straight resulted in elements with lengths about twice those of the myocardial model. With the myocardium discretized at roughly 250 μm resolution, some Purkinje cells could be over 400 μm long. Using only a linear approximation to the potential over an element might not properly capture the potential fields when the length constant is on the order of 100 μm, but a cubic approximation will do a much better job. Sharing the nodes between the two systems, Purkinje and myocardium, was not necessary, but made bookkeeping much easier. Transferring quantities between the two grids was trivial this way, but more nodes could easily be added to the Purkinje system to reduce the element length, at the extra expense of interpolation from the myocardial grid onto the Purkinje grid.

Several models of the Purkinje system have been used in studies, but this is the most complete to date. There have been studies which only considered straight, isolated, unbranching strands subject to electric fields [5], [26], [27]. Interaction with ventricular tissue has also been studied, but in a geomtrically simple model without field effects [22]. More geometrically realistic Purkinje networks have been developed, but only used to study propagation in an isolated tree [18], or been unsuitable for extracellular stimulation due to right-angled bends [12].

The disadvantages of using cubic Hermite elements are that 1) the system to be solved is twice as large as with linear elements, because at each node, current is tracked as well as voltage, and 2) symmetry is lost in the finite element matrices when element lengths are nonuniform since only the shape functions associated with the derivative are dependent on the element length. However, these disadvantages do not impose a large penalty on solving the system due to its relatively small size. For the example tree shown, there are only 851 nodes which resulted in finite element matrices with 10 904 nonzero entries. Such a system can be easily and efficiently solved by a direct LU decomposition. Using linear elements results in approximately one quarter of the nonzero entries (2487) and faster computation, but any decrease in the computation time of the Purkinje system is unnoticed since solving the bulk myocardium requires orders of magnitude more time. The solution obtained with the cubic Hermite elements is also more accurate, since it also tries to minimize the error in the current.

The model of the Purkinje displays sawtooth effects which are dependent on the physical parameters chosen and the field applied. It can be used to excite a finite element model of the myocardium with a resultant excitation pattern similar to those recorded [16]. One great advantage of the model is its ability to easily simulate conditions like bundle branch block. One need merely interrupt the Purkinje network at the appropriate place to observe the change in activation.

B. Sawtooth Effects

The sawtooth effect has long been hypothesized but never seen on the organ level. If it is to play a prominent role anywhere, the Purkinje system seems to offer the greatest promise. The Purkinje system is 1-D, and, thus, there will not be an averaging effect as has been described with tissue [9]. Even the large bundles of the Purkinje fibers, forming the left and right bundle branches, seem to be more of a collection of individual fibers than one large syncytial trunk, since transverse connections were found to be very rare [28]. This arrangement will promote the formation of sawtooth potentials. However, further investigation is needed to better quantify the degree of lateral coupling since evidence of good coupling has also been presented [29].

Sawtooth effects do not seem to be the prominent mechanism for exciting the fibers far from the stimulus, especially for uniform fields. Rather, the curves and terminal ends of the Purkinje system play a greater role in creating secondary sources. The sawtooth effect is smaller, superimposed on top of the larger response. It can extend the directly excited region, as evidenced by shorter activation times, by pushing near threshold regions just outside the directly excited region above threshold. With a nonuniform field, midcable excitation was also possible. When the isolated tree was considered, sawtooth effects caused a significant shortening of activation time when the gap junction resistance was increased for a field in the x-direction. While the sawtooth effect alone may not lead to excitation, it will contribute to a greater region being excited, which may be significant due to the nonlinear nature of the system.

Krassowska and Kumar [30] reject the importance of the sawtooth effect in causing far field stimulation based on a series of simulations performed on a membrane patch, single cell, and fiber. It must be noted that they did not simulate a model with discrete junctions so they had to infer their conclusion. They based it on single cell considerations, noting that the threshold for a single cell was 6.9 V/cm, a very large field. However, that assumed that the cell was at resting voltage. As shown in Fig. 4, increasing the gap junction resistance changed the baseline, creating a hump in the middle of the cable. Increasing the field strength (Fig. 3) also increased the baseline over the middle portion of the cable, lowering the sawtooth amplitude necessary for an action potential. The cable used in this simulation was 5 mm long, 2 mm longer than in the Krassowska simulations. With the shorter cable length, end effects would overlap slightly in the middle region depending on the particular conditions, masking true far field effects. With the longer cable used in this simulation, the central region was truly free of end effects as can be seen in Fig. 4 where the baseline in the central region is constant. Finally, excitation distant from the electrode is especially apparent in our simulation with a nonuniform field (see Fig. 4). Krassowska only explored a field with a constant gradient so that may account for part of the discrepancy. For weaker fields,

our results agree with Krassowska in that excitation will start at the ends of the cable.

Many factors affected the amplitude of the sawtooth variation in transmembrane voltage. The nominal value of effective conductivity used, 0.3 S/m, results in a longitudinal cellular resistance of 1.3 $\mathrm{M}\Omega$ for a 100 $\mu\mathrm{m}$ cell. Thus, junctional resistances much below this do not lead to large sawtooth variations since the junctional discontinuity is not great compared to the drop in potential along the length of the cell. This is evidenced in both Fig. 3(b) and Fig. 4 where large effects are not seen until either the cell resistance drops to the gap junction resistance, as in the former figure, or the gap junctional resistance increases to the cellular resistance, as in the latter figure. This is also in agreement with experimental results which showed an increase in the sawtooth amplitude when the coupling resistance was increased by exposure to heptanol [8]. Increasing just the gap junction resistance does not increase the sawtooth amplitude linearly since, although the resistance is larger between cells, less intracellular current flows due to the increased resistance.

Gillis *et al.* [9] found no evidence of sawtooth potentials when they subjected strands of cultured monolayers of rat neonatal myocytes to extracellular electric field stimulation. This may be explained by the gap junction distribution of neonatal cells, which are distributed along the edges of the cells as opposed to being concentrated at the ends [31]. This distribution of gap junctions is very different from Purkinje strands found in human branch bundles, which display very few lateral connections [28]. Also, while the cells on the borders of the cell mask followed the border, interior cells were more distributed in their orientation. Thus, these two factors may combine to increase the lateral averaging effect [32] in the experimental setup of Gilles *et al.*. In contrast, Tung's group [8] found unambiguous sawtooth potentials, in agreement with theory, in their two cell preparation. High resolution optical mapping of the Purkinje system voltage response is ultimately needed to resolve the issue.

C. Role in Defibrillation

During defibrillation shocks, the role of the Purkinje remains unelucidated. Even though it resides on the endocardium, its response to an electric shock will be very different form that of the myocardium. It is isolated from the myocardium as well as being a 1-D structure. As such, the changes in conductivity with respect to the electric field will be much different from that of the myocardium. It can be expected that the spatially complex electric field produced by a defibrillation shock will lead to rapid excitation of the Purkinje system. Since the Purkinje activates the myocardium, this can have great impact on the development of the post-shock activity. For example, activity from the Purkinje System can emanate from a PMJ and serve to consume an excitable gap, thus terminating a potential rotor. Conversely, activity from a PMJ may interact with refractory tissue to create a wavebreak.

Based on results from a straight cable exposed to a non-uniform field, and the full network exposed to a uniform field, the Purkinje system will activate very quickly. With a straight fiber exposed to a uniform field, excitation only occurred at the cable ends. With a nonuniform field, excitation could be initiated in the middle of the cable. This led to a much more rapid excitation of the entire cable, as well as excitation far from the electrode. While other studies investigating the sawtooth effect have imposed nonuniform surface to volume ratios, conductivities, cell length, and extracellular space [27], [33], this study is the first to demonstrate that a nonuniform field is sufficient for the sawtooth effect to cause excitation far from the electrode. The field produced by a defibrillatory device, either implanted or external, will certainly be highly nonuniform.

As explained by Sobie *et al.* [1] in a mathematical analysis of the bidomain equations, activation of cardiac tissue depends on a field gradient, the divergence of the conductivity, and the relative orientations of each. The conductivity of the Purkinje system is defined by the cable direction. Since the strands of the Purkinje run in many different directions over the endocardial surface, a portion of the network will always be in position to be stimulated by an external field. The direction in which a Purkinje strand runs is not correlated with the direction of the myocardial fibers on which it runs, so the Purkinje strand will experience a different excitation than the myocardium. Thus, a defibrillation shock will create different spatial patterns of deexcitation in the Purkinje system and myocardium. Activity from the myocardium may even move retrogradely into the Purkinje system [34] further complicating the defibrillation process. Activity from the Purkinje system will only move into the myocardium, and vice versa, if tissue in the other system is deexcited when the activation reaches the PMJ. A more exhaustive study with more realistic extracellular fields and full ventricles is required to ascertain the effect of the rapid, nonuniform Purkinje activation on defibrillation.

D. Limitations

The Purkinje system constructed is not created from a detailed analysis of one biological specimen. It has a much finer structure than that given here. Refinement of the ends of the network is an ongoing project. Regardless, activation profiles are fit well with the present network.

Many physical attributes of the His/Purkinje system are still unknown. The best representation of Purkinje membrane dynamics are over two decades old, and, hence, do not incorporate the latest descriptions and findings. Results depend on the exact physical parameters such as cell geometry. However, cells comprising the Purkinje network can show a great variability in dimensions [28]. The value of the gap junction resistance is unknown. Estimates for myocardium based upon experiments range from 1 $\mathrm{M}\Omega$ [35] to tens of $\mathrm{M}\Omega$ [32]. The gap junction resistances of the Purkinje system should be smaller than those of the myocardium because the myocardium primarily uses connexin43 which has a unitary conductance of only 100 pS, while the Purkinje system uses also connexin40 which has a unitary conductance of 215 pS [36].

The Beeler-Reuter ionic model was used for the ventricular membrane dynamics. While such a model is not as complete as current models [37], [38], it is sufficient for the purposes of this particular aspect of the study, namely to demonstrate that the method as described is capable of exciting the myocardium. When reentry and repolarization are to be considered, a better model will be selected.

V. Conclusion

The Purkinje system is distinct from the bulk ventricular myocardium. It has different electrophysiological properties, as well as different geometrical properties, making its response to extracellular stimuli distinct from that of the myocardium. The curving geometry and numerous endings of the Purkinje system lead to multiple sites of field activation. Due to the 1-D nature of the Purkinje system, it is more vulnerable to the sawtooth effect. Under certain conditions, this may be of significance and affect excitation patterns resulting from defibrillation strength shocks. How defibrillation success is altered by the presence of the Purkinje system requires further analysis in a complete ventricular model.

Appendix

Cubic Hermite elements are defined by two nodes separated by distance L, with each node having two shape functions associated with it. At each node, one shape function defines the potential at that node, and the other defines the gradient of the potential. The four shape functions are as follows:

$$\alpha_1(\xi) = 1 - 3\xi^2 + 2\xi^3 \tag{12}$$
$$\alpha_2(\xi) = \xi(\xi - 1)^2 \tag{13}$$
$$\alpha_3(\xi) = \xi^2(3 - 2\xi) \tag{14}$$
$$\alpha_4(\xi) = \xi^2(\xi - 1). \tag{15}$$

The potential within an element, defined by nodes at x_1 and x_2, is given by

$$\phi(\xi) = \alpha_1(\xi)\phi(x_1) + \alpha_2(\xi)\frac{\partial\phi(x_1)}{\partial\xi} + \alpha_3(\xi)\phi(x_2) + \alpha_4(\xi)\frac{\partial\phi(x_2)}{\partial\xi}. \tag{16}$$

However, it is desired to use the longitudinal current, i_L, instead of the gradient in local coordinates. Thus, the local coordinates must be converted to global units so that current can be used. Recalling that

$$i_L = -\sigma_i^*\pi\rho^2\frac{\partial\phi(x)}{\partial\xi}\frac{\partial\xi}{\partial x} \tag{17}$$
$$= -\frac{\sigma_i^*\pi\rho^2}{L}\frac{\partial\phi(x)}{\partial\xi} \tag{18}$$

with the equivalent conductivity computed from

$$\sigma_i^* = \frac{\sigma_i L}{L + \sigma_i r_{gj}\pi\rho^2} \tag{19}$$

The stiffness matrix is then calculated from

$$K_{ij} = \int_\Omega k(j)\frac{\partial\alpha_i}{\partial\xi}\frac{\partial\alpha_j}{\partial\xi}d\Omega' \tag{20}$$

with

$$k(j) = \begin{cases} -\sigma_i^*\pi\rho^2, & \text{j odd} \quad (21a) \\ \frac{1}{L}, & \text{j even} \quad (21b) \end{cases}$$

and the mass matrix by

$$M_{ij} = \int_\Omega m(j)\alpha_i\alpha_j d\Omega' \tag{22}$$

with

$$m(j) = \begin{cases} -\frac{1}{\pi\rho^2\sigma_i^*}, & \text{j odd} \quad (23a). \\ 1, & \text{j even} \quad (23b) \end{cases}$$

The vector to be solved for each element is now expressed in terms of potential and longitudinal current at the nodes

$$[\phi(x_1) i_L(x_1) \phi(x_2) i_L(x_2)]^T. \tag{24}$$

In summary

1) $$V_m^t = f_1\left(\phi_i^t, \phi_e^t, i_L^t\right) \tag{25}$$
2) $$\bar{\zeta}^{t+1} = f_{\text{ion}}\left(V_m^t, \bar{\zeta}^t\right) \tag{26}$$
$$V_m^{t+1/2} = f_2\left(V_m^t, \bar{\zeta}^{t+1}\right) \tag{27}$$
3) $$\phi_i^{t+1/2} = f_3\left(V_m^{t+1/2}, \phi_e^t\right) \tag{28}$$
$$i_L^{t+1/2} = f_4\left(V_m^{t+1/2}\right) \tag{29}$$
4) $$\left\{\phi_i^{t+1}, i_L^{t+1}\right\} = f_5\left(\phi_i^{t+1/2}, i_L^{t+1/2}, \phi_e^t, \phi_e^{t-1}\right) \tag{30}$$

where f_1–f_5 are given by (3)–(6), and (8) respectively, and f_{ion} is ionic model dependent.

References

[1] E. Sobie, R. Susil, and L. Tung, "A generalized activating function for predicting virtual electrodes in cardiac tissue," *Biophys. J.*, vol. 73, no. 3, pp. 1410–1423, 1997.

[2] W. Han, W. Bao, Z. Wang, and S. Nattel, "Comparison of ion-channel subunit expression in canine cardiac Purkinje fibers and ventricular muscle," *Circ. Res.*, vol. 91, no. 9, pp. 790–797, 2002.

[3] T. Stankovicova, V. Bito, F. Heinzel, K. Mubagwa, and K. R. Sipido, "Isolation and morphology of single Purkinje cells from the porcine heart," *Gen. Physiol. Biphys.*, vol. 22, no. 3, pp. 329–340, 2003.

[4] H. G. Li, D. L. Jones, R. Yee, and G. J. Klein, "Defibrillation shocks produce different effects on Purkinje fibers and ventricular muscle: implications for successful defibrillation, refibrillation and postshock arrhythmia," *J Am. Coll. Cardiol.*, vol. 22, no. 2, pp. 607–614, 1993.

[5] R. Plonsey and R. C. Barr, "Effect of microscopic and macroscopic discontinuities on the response of cardiac tissue to defibrillating (stimulating) currents," *Med. Biol. Eng. Comput.*, vol. 24, no. 2, pp. 130–136, 1986.

[6] W. Krassowska, T. C. Pilkington, and R. E. Ideker, "Periodic conductivity as a mechanism for cardiac stimulation and defibrillation," *IEEE Trans. Biomed. Eng.*, vol. BME-34, pp. 555–559, 1987.

[7] N. Trayanova and T. C. Pilkington, "A bidomain model with periodic intracellular junctions: a one-dimensional analysis," *IEEE Trans. Biomed. Eng.*, vol. 40, no. 5, pp. 424–433, May 1993.

[8] V. Sharma and L. Tung, "Theoretical and experimental study of sawtooth effect in isolated cardiac cell-pairs," *J. Cardiovasc. Electrophysiol.*, vol. 12, no. 10, pp. 1164–1173, 2001.
[9] A. Gillis, V. Fast, S. Rohr, and A. Kleber, "Spatial changes in transmembrane potential during extracellular electrical shocks in cultured monolayers of neonatal rat ventricular myocytes," *Circ. Res.*, vol. 79, no. 4, pp. 676–690, 1996.
[10] T. Argentieri, L. Frame, and T. Colatsky, "Electrical properties of canine subendocardial Purkinje fibers surviving in 1-day-old experimental myocardial infarction," *Circ. Res.*, vol. 66, no. 1, pp. 123–134, 1990.
[11] A. Pollard and R. Barr, "The construction of an anatomically based model of the human ventricular conduction system," *IEEE Trans. Biomed. Eng.*, vol. 37, no. 12, pp. 1173–1185, Dec. 1990.
[12] O. Berenfeld and J. Jalife, "Purkinje-muscle reentry as a mechanism of polymorphic ventricular arrhythmias in a 3-dimensional model of the ventricles," *Circ. Res.*, vol. 82, pp. 1063–1077, 1998.
[13] F. Vetter and A. McCulloch, "Three-dimensional analysis of regional cardiac function: a model of rabbit ventricular anatomy," *Prog. Biophys. Mol. Biol.*, vol. 69, no. 2–3, pp. 157–183, 1998.
[14] G. Zigelman, R. Kimmel, and N. Kiryati, "Texture mapping using surface flattening via multidimensional scaling," *IEEE Trans. Vis. Comput. Graph.*, vol. 8, no. 2, pp. 98–207 **<Au: Confirm page range?>**, Apr.-Jun. 2002.
[15] R. Gould, *Graph Theory*. Don Mills, ON, Canada: Benjamin/Cummings, 1988.
[16] D. Durrer, R. T. van Dam, G. E. Freud, M. J. Janse, F. L. Meijler, and R. C. Arzbaecher, "Total excitation of the isolated human heart," *Circulation*, vol. 41, pp. 899–912, 1970.
[17] F. H. Netter, *Atlas of Human Anatomy*, 2nd ed. East Hanover, NJ: Novartis, 1997.
[18] A. E. Pollard and R. C. Barr, "The construction of an anatomically based model of the human ventricular conduction system," *IEEE Trans. Biomed. Eng.*, vol. 37, no. 12, pp. 1173–1185, Dec. 1990.
[19] K. Simelius, J. Nenonen, and M. Horáček, "Modeling cardiac ventricular activation," *Int. J. Bioelectromag.*, vol. 3, pp. 51–58, 2001.
[20] D. DiFrancesco and D. Noble, "A model of cardiac electrical activity incorporating ionic pumps and concentration changes," *Philos. Trans. Roy. Soc. Lond. B. Biol. Sci.*, vol. 307, no. 1133, pp. 353–398, 1985.
[21] D. Huelsing, K. Spitzer, J. Cordeiro, and A. Pollard, "Conduction between isolated rabbit Purkinje and ventricular myocytes coupled by a variable resistance," *Am. J. Physiol.*, vol. 274, no. 4, pt. 2, pp. H1163–H1173, 1998.
[22] M. Monserrat, J. Saiz, J. Ferrero, Jr, J. Ferrero, and N. Thakor, "Ectopic activity in ventricular cells induced by early afterdepolarizations developed in Purkinje cells," *Ann. Biomed. Eng.*, vol. 28, no. 11, pp. 1343–1351, 2000.
[23] A. Hodgkin, "A note on conduction velocity," *J. Physiol. (Lond.)*, vol. 125, pp. 221–224, 1954.
[24] J. P. Drouhard and F. A. Roberge, "Revised formulation of the Hodgkin-Huxley representation of the sodium current in cardiac cells," *Comput. Biomed. Res.*, vol. 20, no. 4, pp. 333–350, 1987.
[25] R. Wiedmann, R. Tan, and R. Joyner, "Discontinuous conduction at Purkinje-ventricular muscle junction," *Am. J. Physiol.*, vol. 271, no. 4, pt. 2, pp. H1507–H1516, 1996.
[26] R. Plonsey and R. C. Barr, "Inclusion of junction elements in a linear cardiac model through secondary sources: application to defibrillation," *Med. Biol. Eng. Comput.*, vol. 24, pp. 137–144, 1986.
[27] W. Krassowska, "Field stimulation of cardiac fibers with random spatial structure," *IEEE Trans. Biomed. Eng.*, vol. 50, no. 1, pp. 33–40, Jun. 2003.
[28] P. R. Vassall-Adams, "Ultrastructure of the human atrioventricular conduction tissues," *Eur. Heart J.*, vol. 4, no. 7, pp. 449–460, 1983.
[29] S. Weidmann, "The electrical constants of Purkinje fibres," *J. Physiol.*, vol. 118, no. 3, pp. 348–360, 1952.
[30] W. Krassowska and M. Kumar, "The role of spatial interactions in creating the dispersion of transmembrane potential by premature electric shocks," *Ann. Biomed. Eng.*, vol. 25, no. 6, pp. 949–963, 1997.
[31] R. H. Hoyt, M. L. Cohen, and J. E. Saffitzc, "Distribution and three-dimensional structure of intercellular junctions in canine myocardium," *Circ. Res.*, vol. 64, no. 3, pp. 563–574, 1989.
[32] V. Fast and A. Kleber, "Microscopic conduction in cultured strands of neonatal rat heart cells measured with voltage-sensitive dyes," *Circ. Res.*, vol. 73, no. 5, pp. 914–925, 1993.
[33] M. Fishler, "Syncytial heterogeneity as a mechanism underlying cardiac far-field stimulation during defibrillation-level shocks," *J. Cardiovasc. Electrophysiol.*, vol. 9, no. 4, pp. 384–394, 1998.
[34] R. Gilmour, Jr and M. Watanabe, "Dynamics of circus movement re-entry across canine Purkinje fibre-muscle junctions," *J. Physiol.*, vol. 476, no. 3, pp. 473–485, 1994.
[35] R. Chapman and C. Fry, "Estimation of the resistance of the intercalated disk in the ventricle of the frog Rana pipiens," *J. Physiol.*, vol. 244, no. 1, pp. 34P–35P, 1975.
[36] S. Elenes, M. Rubart, and A. P. Moreno, "Junctional communication between isolated pairs of canine atrial cells is mediated by homogeneous and heterogeneous gap junction channels," *J. Cardiovasc. Electrophysiol.*, vol. 10, no. 7, pp. 990–1004, 1999.
[37] T. R. Shannon, F. Wang, J. Puglisi, C. Weber, and D. M. Bers, "A mathematical treatment of integrated Ca dynamics within the ventricular myocyte," *Biophys. J.*, vol. 87, no. 5, pp. 3351–3371, 2004.
[38] V. Iyer, R. Mazhari, and R. L. Winslow, "A computational model of the human left-ventricular epicardial myocyte," *Biophys. J.*, vol. 87, no. 3, pp. 1507–1525, 2004.

Edward J. Vigmond (S'96–M'97) received the B.A.Sc. degree in electrical and computer engineering from the University of Toronto, Toronto, ON, Canada, in 1988. He received the M.A.Sc. and Ph.D. degrees from the Institute of Biomedical Engineering, University of Toronto in 1991 and 1996, respectively.

He is currently an Associate Professor with the Department of Electrical and Computer Engineering, University of Calgary, Calgary, AB, Canada, where he is modeling biological electrical activity. Prior to this, he was a Postdoctoral fellow at the University of Montreal ('97–'99) and Tulane University ('99–'01). His research interests include numerical computation of electrical fields, biomedical signal processing, and modeling of nonlinear biosystems.

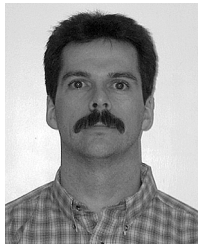

Clyde Clements received the B.Sc. degree in applied mathematics from Memorial University of Newfoundland, NF, Canada. He also received the M.Sc. degree in mathematics and the Ph.D. degree in physiology and biophysics from Dalhousie University, Halifax, NS, Canada.

He completed a Postdoctoral position in the Department of Electrical and Computer Engineering at the University of Calgary, Calgary, AB, Canada, in 2006. His main research interests are mathematical and computational modelling of cardiac electrophysiology.